# CrRLK1L receptor-like kinases HERK1 and ANJEA are female determinants of pollen tube reception

Sergio Galindo-Trigo[1], Noel Blanco-Touriñán[2], Thomas A. DeFalco[3,4], Cyril Zipfel[3,4], Julie E Gray[5], Lisa M Smith[1*]

[1]Department of Animal and Plant Sciences, University of Sheffield, Western Bank, Sheffield S10 2TN, UK

[2]Instituto de Biología Molecular y Celular de Plantas, Consejo Superior de Investigaciones Científicas, Universidad Politécnica de Valencia, Valencia, Spain

[3]The Sainsbury Laboratory, Norwich Research Park, Norwich NR4 7UH, UK

[4]Department of Molecular and Cellular Plant Physiology, University of Zurich, Zollikerstrasse 107, CH-8008 Zurich, Switzerland

[5]Department of Molecular Biology and Biotechnology, University of Sheffield, Western Bank, Sheffield S10 2TN, UK

*Corresponding author: lisa.m.smith@sheffield.ac.uk

## Abstract

Communication between the male and female gametophytes is vital for fertilisation to occur in angiosperms. A number of receptor-like kinases have been implicated in male-female interactions. Notably, the CrRLK1L family proteins ANX1, ANX2, BUPS1 and BUPS2 are required to prevent pollen tube burst before fertilisation, while the CrRLK1L protein FER is required for pollen tube burst upon entrance into the female gametophyte. Here, we show that two further CrRLK1L proteins act redundantly to control pollen tube burst at the female synergid cell. In the absence of HERK1, which also functions in cell elongation in leaves, and its previously uncharacterized homologue ANJEA, the majority of ovules are not fertilised due to pollen tube overgrowth. Both proteins are localised to the filiform apparatus of the synergid cells in the unfertilised ovule and act as female determinants for fertilisation. As in *fer* mutants, the synergid cell-specific, endomembrane protein NTA is not relocalised after pollen tube reception; however reactive oxygen species levels are not affected in *herk1 anj* double mutants. ANJEA and HERK1 interact directly with LRE, a glycosyl-phosphatidylinositol-anchored protein proposed to act as co-receptor for FER at the filiform apparatus. Our results support that HERK1 and ANJEA can form receptor complexes with LRE at the filiform apparatus to mediate female-male gametophyte interactions during plant fertilisation.



## Keywords

CrRLK1L, Fertilisation, Synergid, Receptor Kinase, Angiosperm

## Author summary

We depend on seeds for food and to sustain our livestock. Seed production relies on efficient plant sexual reproduction, which in turn requires the coordination of male and female gametes during fertilisation. Using reverse genetics and the model flowering plant *Arabidopsis thaliana,* we have identified two novel regulators of fertilisation. The receptors HERK1 and ANJEA act in the maternal tissues to ensure the timely release of the male gametes from the pollen tube into the female ovule, a necessary step for successful fertilisation. Our work assigns two additional receptors to the toolbox that controls early stages of fertilisation, therefore expanding our current knowledge of the regulation of plant reproduction in flowering plants. These findings will be a useful underpinning for future research aiming to understand the molecular basis of the signalling events that lead to fertilisation and, as a consequence, seed production.

65 ## Introduction

66 Fertilisation is a critical point in the life cycle of any sexually reproducing organism. In flowering
67 plants, gametes are enclosed in gametophytes, multicellular structures that develop in the
68 reproductive organs of the flower. The pollen grain constitutes the male gametophyte, with each
69 grain generating a pollen tube in the form of a rapidly growing cellular protrusion that delivers the
70 male gametes, or sperm cells, into the ovule. Female gametophytes develop inside the ovule and
71 contain the female gametes within an embryo sac; the egg cell and central cell. The process of
72 double fertilisation in angiosperms consists of the fusion of a sperm cell with each of the female
73 gametes. If fertilisation is successful, the embryo and endosperm develop from the egg cell and
74 central cell fertilisations, respectively. For double fertilisation to occur, the male and female
75 gametophytes must engage in a molecular dialog that controls pollen tube attraction towards the
76 ovule entrance, or micropyle, the arrest of pollen tube growth and the release of the sperm cells
77 within the ovule (see (1) for a detailed review).

78 The synergid cells occupy the micropylar portion of the female gametophyte, and their function is
79 strongly linked to communication between the gametophytes. As such, their cytoplasm is densely
80 occupied by endomembrane compartments, reflective of a highly active secretion system
81 generating messenger molecules (2). The filiform apparatus appears at the outermost pole, a
82 thickened and intricate cell wall structure that represents the first contact point between female and
83 male gametophytes prior to fertilisation (3). Synergid cells secrete small cysteine-rich LURE
84 peptides to guide pollen tubes towards the embryo sac (4). LURE peptides are sensed by two
85 pairs of pollen-specific receptor-like kinases (RLKs), MALE DISCOVERER 1 (MDIS1) and MDIS1-
86 INTERACTING RLK 1 (MIK1), and POLLEN-SPECIFIC RECEPTOR KINASE 6 (PRK6) and PRK3
87 in Arabidopsis (5, 6). These RLKs bind LURE peptides through their extracellular domains at the
88 growing tip of the pollen tubes, triggering directional growth towards the synergid cells (5-7).

89 Within the expanded family of RLKs in Arabidopsis, the *Catharanthus roseus* RLK1-like (CrRLK1L)
90 subfamily has been linked to several aspects of fertilisation. Two pairs of functionally redundant
91 CrRLK1Ls are integral in controlling pollen tip growth [ANXUR1 and 2 (ANX1/2), and BUDDHA'S

92 PAPER SEAL 1 and 2 (BUPS1/2) (8-10)]. ANX1/2 and BUPS1/2 heterodimerise and ensure pollen
93 tube growth by sensing of two autocrine secreted peptides belonging to the RAPID
94 ALKALINIZATION FACTOR (RALF) family, RALFL4 and RALFL19 (9, 11). A fifth CrRLK1L
95 protein, ERULUS (ERU), has also been implicated in male-determined pollen tube growth via
96 regulation of $Ca^{+2}$ oscillations (12). The CrRLK1L protein FERONIA (FER) accumulates in the
97 filiform apparatus of the synergids and functions as a female determinant of pollen tube burst and
98 subsequent sperm cell release (13, 14). Although no extracellular ligand has been identified for
99 FER in a reproductive context, there is evidence for FER activation of a synergid-specific signalling
100 cascade upon pollen tube arrival. This signalling pathway involves the glycosyl-phosphatidylinositol
101 (GPI)-anchored protein LORELEI (LRE) (15), activation of NADPH oxidases to generate reactive
102 oxygen species (ROS) in the micropyle (16), generation of specific $Ca^{2+}$ signatures in the synergid
103 cytoplasm (17), and relocalisation of the Mildew resistance locus O (MLO)-like NORTIA (NTA), an
104 endomembrane compartment protein that affects pollen tube-induced $Ca^{2+}$ signatures in the
105 synergids (17-19).

106 Many questions remain about the nature of the communication between gametophytes that
107 controls sperm cell release and CrRLK1Ls FER, ANX1/2 and BUPS1/2 are potential receptor
108 candidates to mediate this dialog. Here we report the characterisation of CrRLK1Ls HERCULES
109 RECEPTOR KINASE 1 (HERK1) and ANJEA (AT5G59700; ANJ) as female determinants of pollen
110 tube reception in Arabidopsis. HERK1 and ANJ act redundantly at the filiform apparatus of the
111 synergids to control pollen tube growth arrest and burst, representing two new mediators of
112 gametophytic communication and therefore expanding the female-specific toolbox required for
113 fertilisation.

## 114 Results

### 115 HERK1 and ANJEA function redundantly in seed set

116 To test whether additional Arabidopsis CrRLK1L proteins are involved in reproduction, we obtained
117 T-DNA insertion lines for all seventeen family members. Presence of a homozygous insertion was

118 verified for ten CrRLK1L genes. These verified lines were crossed and double homozygous plants
119 selected in the F2 generation by PCR genotyping (Figure S1A-B for T-DNA lines used further in
120 this study). Stable double homozygous lines were examined for reduced fertility. Through this
121 screen, we identified that double mutants in *HERCULES RECEPTOR KINASE 1 (HERK1)* and
122 *AT5G59700* (hereafter referred to as *ANJEA/ANJ*) have high rates of unfertilised ovules or seeds
123 that have aborted very early in development, and shorter siliques (Figure 1A). HERK1 and ANJEA
124 are close homologues within the CrRLK1L family (20), with 75% identity and 86% similarity at the
125 protein level. Loss of *ANJ* gene expression in the double homozygous *herk1-1 anj-1* T-DNA line
126 (hereafter referred to as *herk1 anj*) was confirmed by RT-PCR (Figure S1C), with the *herk1-1* T-
127 DNA insertion previously confirmed to knockout gene expression (21).

128 To verify that the low rate of seed set results from functional redundancy between *HERK1* and
129 *ANJ*, we examined seed development in dissected siliques of wild-type, *herk1*, *anj* and *herk1 anj*
130 plants grown in parallel. While single mutants *herk1* and *anj* did not have elevated numbers of
131 unfertilised/aborted seeds compared to wild-type, a high proportion of ovules in *herk1 anj* siliques
132 had not developed into mature seeds, leading to a reduced number of seeds per silique (Figure
133 1B). Therefore we conclude that there is functional redundancy between the HERK1 and ANJ
134 proteins during fertilisation or early seed development.

135 HERK1 has previously been described to influence cell elongation in vegetative tissues with
136 THESEUS1 and HERK2, with the *herk1 the1-4* and *herk1 herk2 the1-4* mutants displaying a short
137 petiole phenotype, similarly to *fer* mutants (21, 22). We further examined the *herk1 anj* mutants for
138 developmental defects in vegetative and reproductive growth, finding no further developmental
139 aberrations (Figure S2A-G). Thus, HERK1 and ANJ do not act redundantly during vegetative
140 growth.

141 **HERK1 and ANJEA are female determinants of pollen tube burst**

142 Previous studies of CrRLK1L proteins where mutation results in low or absent seed set have
143 identified functions in pollen tube growth (ANX1, ANX2, BUPS1, BUPS2 and ERU; (8-12)) and

144 female-mediated pollen tube burst at the synergids (FER (14)). To test which step in fertilisation is
145 impaired in the *herk1 anj* mutant, we tracked pollen tube growth through the style in single and
146 double mutants. In all plant lines, aniline blue staining revealed that the pollen tubes targeted the
147 female gametophytes correctly (Figure S3). However, closer examination of the ovules revealed
148 pollen tube overgrowth at high frequency in *herk1 anj* mutants. While pollen tube overgrowth is
149 rare in wild-type and single mutants, 83% of pollen tubes failed to burst upon entering ovules in the
150 double mutant (Figure 1C). The 83% of ovules exhibiting pollen tube overgrowth is notably higher
151 than the 71% of ovules that fail to develop into seeds (Figure 1B,C), indicating that in some cases
152 fertilisation occurs in the presence of pollen tube overgrowth. Pollen tube overgrowth in *herk1 anj*
153 is occasionally accompanied by polytubey, where more than one pollen tube enters the ovule, as
154 reported for several other mutations causing pollen tube overgrowth including *fer* (Figure S4A-B;
155 (13, 23)). This is indicative of uninterrupted secretion of attraction signals from the synergid cells,
156 suggesting impaired degeneration of the receptive synergid cell upon pollen tube arrival (24, 25).

157 In *fer* mutants, pollen tube overgrowth occurs due to maternal defects in male-female gametophyte
158 communications (13, 14, 16). To confirm that HERK1 and ANJ are female determinants of pollen
159 tube burst, we performed reciprocal crosses between the *herk1 anj* mutant and wild-type plants, as
160 well as control crosses within each plant line. While wild-type Col-0 (female; f) x *herk1 anj* (male;
161 m) crosses resulted in 1% of ovules with pollen tube overgrowth, over 90% of pollen tubes
162 exhibited overgrowth in *herk1 anj* (f) x wild-type (m) crosses, indicating that pollen tube overgrowth
163 is a maternally-derived phenotype in *herk1 anj* mutants (Figure 1D). As expected, pollen tube
164 overgrowth was observed in only 3% of the ovules in the control wild-type (f) x wild-type (m)
165 crosses, while 89% of ovules had overgrowth of the pollen tube in *herk1 anj* (f) x *herk1 anj* (m)
166 crosses.

167 To confirm that the reproductive defect is due to the disruption of the *HERK1* and *ANJ* genes and
168 not to additional T-DNA insertions, we re-introduced the *HERK1* and *ANJ* genes into the *herk1 anj*
169 background to test for complementation of the pollen tube overgrowth phenotype. We generated
170 *pHERK1::HERK1* and *pANJ::ANJ-GFP* constructs and obtained *pFER::HERK1-GFP* (26). A
171 *pBRI1::HERK1-GFP* construct has previously been used to complement the *herk1* mutant (21),

172 and we found that while *pHERK1::HERK1* could be generated, *pHERK1::HERK1-GFP* could not
173 be cloned due to toxicity in several bacterial strains. In the developing ovules of five independent
174 T1 plants where a hemizygous insertion would segregate 50:50, expression of *pFER::HERK1-GFP*
175 or *pANJ::ANJ-GFP* constructs in the *herk1 anj* background reduced pollen tube overgrowth by
176 ~50%, as did a *pHERK1::HERK1* construct (Figure S5A). Complementation indicates that these
177 reporter constructs produce functional proteins and confirms that the T-DNA insertions in the
178 *HERK1* and *ANJ* genes are responsible for pollen tube overgrowth. We conclude that HERK1 and
179 ANJ are female determinants of pollen tube burst and therefore named *AT5G59700* after the
180 fertility goddess in Australian aboriginal mythology, Anjea.

181 The kinase activity of FER is not required for its control of pollen tube reception in ovules (26). We
182 therefore tested for complementation of the *herk1 anj* reproductive defect with kinase-dead (KD)
183 versions of HERK1 and ANJ generated by targeted mutagenesis of key residues within the kinase
184 activation loop (D609N/K611R for HERK1 and D606N/K608R for ANJ; (27)). *pHERK1::HERK1-KD*
185 and *pANJ::ANJ-KD-GFP* were also able to complement the pollen overgrowth phenotype,
186 indicating that the kinase activity of these RLKs is not required for their function in fertilisation
187 (Figure S5B). The similarity in the mutant phenotypes, cellular localisation and the dispensable
188 kinase activity in HERK1/ANJ and FER suggests they may act in the same signalling pathway as
189 co-receptors or as parallel receptor systems.

## 190 HERK1 and ANJEA are localised to the filiform apparatus

191 We generated *promoter::GUS* (β-glucuronidase) transcriptional fusions to gain insight into the
192 possible function of HERK1/ANJ in fertilisation. Both *HERK1* and *ANJ* are strongly expressed in
193 ovules, specifically along the funiculus and the synergid cell area (Figure 2A-B). *pHERK1::GUS* is
194 also expressed in the style, ovary walls and stamens (Figure 2C and Figure S6A-B), whereas
195 *pANJ::GUS* expression is detected in stigmas and stamens (Figure 2D and Figure S6D-E). No
196 expression was detected in pollen grains within mature anthers, although HERK1 is expressed in
197 some developing pollen grains (Figure S6A,C,F). Thus *HERK1* and *ANJ* are expressed in multiple
198 reproductive tissues, with the pattern of expression suggesting the fertilisation defect may arise

199 through a biological function in the junction of the stigma and style, at the funiculus or in the female
200 gametophyte where *HERK1* and *ANJ* gene expression overlaps.

201 To examine HERK1 and ANJ expression and cellular localisation in ovules, we used the
202 *pANJ::ANJ-GFP* and *pFER::HERK1-GFP* constructs that complement the fertilisation phenotype.
203 Examination of fluorescent signal from HERK1-GFP and ANJ-GFP fusion protein in the female
204 gametophyte showed that they were strongly localised to the filiform apparatus of the synergid
205 cells (Figure 2E-H). The filiform apparatus is a structure formed by dense folds in the plasma
206 membrane and cell wall where the regulators of fertilisation FER and LRE also localise (14, 23,
207 28). This specific cellular localisation suggests that HERK1 and ANJ could function in the same
208 pathway as FER and LRE. While loss of FER or LRE alone leads to a reproductive defect caused
209 by pollen tube overgrowth in the ovule (14, 23), HERK1 and ANJ are functionally redundant, such
210 that HERK1 and ANJ could act as alternative co-receptors for FER and/or LRE during male-female
211 interactions.

## 212 NORTIA relocalisation after fertilisation is impaired in *herk1 anj* mutants

213 Previous reports point to an interdependence between FER, LRE and NTA in their respective
214 cellular localisations (15, 18). FER only accumulates in the filiform apparatus if functional LRE is
215 present, and NTA relocalisation towards the filiform apparatus upon pollen tube arrival is
216 dependent on FER (15, 18). As HERK1 and ANJ may act in the same signalling pathway as FER,
217 we tested whether these two receptors also interfere in this signalling network by studying the
218 localisation of fluorescence-tagged HERK1, ANJ, FER, LRE and NTA in the *herk1 anj* and *lre-5*
219 backgrounds (Figure 3A). Localisation within the synergids of FER-GFP, LRE-Citrine and NTA-
220 GFP was not affected by *herk1 anj* mutations. Similarly, HERK1-GFP and ANJ-GFP localised to
221 the filiform apparatus in the *lre-5* background. Contrary to previous findings (15), under our
222 conditions FER-GFP accumulation in the filiform apparatus was not impaired in *lre-5* plants (n>25;
223 FER-GFP was found at the filiform apparatus in all ovules checked). Therefore, we found no
224 dependency on HERK1/ANJ or LRE for localisation of FER, LRE, HERK1, ANJ or NTA within the
225 synergids.

226 To determine whether NTA relocalisation in synergid cells upon pollen arrival depends on
227 functional HERK1 and ANJ, we transformed *pMYB98::NTA-GFP* into the *herk1 anj* background.
228 Using SR2200-based callose staining to visualise the filiform apparatus and pollen tube, we
229 observed NTA-GFP fluorescence intensity across the length of the synergid cell. In unfertilised
230 ovules, NTA-GFP fluorescence is evenly distributed across the length of the synergid cell in wild-
231 type and *herk1 anj* plants (Figure 3B). Wild-type fertilised ovules have a shift in the fluorescence
232 intensity pattern, with NTA accumulation towards the micropylar end of the synergid cytoplasm and
233 a decrease in relative fluorescence intensity towards the chalazal end (Figure 3B-C). This
234 response is absent in *herk1 anj* fertilised ovules in which the relative fluorescence intensity pattern
235 is indistinguishable from that of unfertilised ovules, indicating a requirement for HERK1/ANJ in
236 NTA relocalisation upon pollen tube perception.

237 As reported by Ngo and colleagues (2014), the journey of the pollen tube does not conclude upon
238 contact with the filiform apparatus of the synergid cells (17). Pollen tubes transiently arrest growth
239 upon contact with the synergid; they then grow rapidly along the receptive synergid and towards
240 the chalazal end, before burst and release of the sperm cells (17). To observe this process in
241 detail, we used TdTomato-tagged pollen and monitored NTA-GFP localisation at different stages of
242 pollen growth within the ovule. The shift in NTA-GFP localisation was noted in ovules in which the
243 pollen tube had grown past the filiform apparatus and ruptured, rather than upon pollen tube arrival
244 at the filiform apparatus (Figure S7A). Interestingly, in rare cases when pollen tube burst occurred
245 normally in the *herk1 anj* background, the fluorescence shift towards the micropyle had also taken
246 place (Figure S7A). In both cases, NTA-GFP did not appear to accumulate in the filiform apparatus
247 (Figure S7B). Our results differ from the interpretation of previous reports that NTA is polarly
248 relocalised from endomembrane compartments to the plasma membrane in the filiform apparatus,
249 instead supporting a more generalised relocalisation within the synergid cytoplasm towards the
250 micropylar end. We propose that HERK1 and ANJ, similarly to FER, act upstream of NTA
251 relocalisation in the signalling pathway. Deciphering whether NTA relocalisation is a requirement or
252 a consequence of pollen tube burst will require the temporal resolution that only high-resolution,
253 live-imaging approaches can provide (17, 29, 30).

254 **ROS production is not affected in mature *herk1 anj* ovules**

255 ROS levels in *fer-4* and *lre-5* ovules have been reported to be significantly lower than in wild-type
256 with the implication that, as hydroxyl free radicals can induce pollen tube burst (16), reduced ROS
257 levels could be responsible for pollen tube overgrowth. To assess whether HERK1 and ANJ also
258 act upstream of ROS accumulation in the ovules, we used $H_2$DCF-DA to measure ROS levels on a
259 categorical scale in *herk1 anj*, *lre-5* and *fer-4* ovules (Figure S8A). In stage 14 flowers (31), when
260 the highest levels of ROS are reported in wild-type ovules (16), we could recapitulate a strong
261 reduction in ROS levels in *fer-4* ovules (16), with a lesser reduction in *lre-5* and *herk1 anj* (Figure
262 S8B).

263 Subsequently, we analysed the female gametophyte structure in *herk1 anj* ovules of stage 14
264 flowers and verified they develop correctly and accumulate callose at the filiform apparatus,
265 suggesting that the observed phenotypes are due to a signalling rather than a morphological
266 defect (Figures 4A and S9A-C; (32)). Undeveloped ovules in the *herk1 anj* mutant could hinder our
267 interpretation of the ROS measurements. Thus, we studied gametophytic development in *herk1*
268 *anj*, *lre-5* and *fer-4* stage 14 flowers at 0 and 20 hours after emasculation (HAE). Quantification of
269 development indicated that at 0 HAE more than 40% of wild-type ovules were not mature, with a
270 further delay in development in *herk1 anj* and *fer-4* ovules (Figure S10A). At 20 HAE, all ovules
271 had reached the mature 7-celled or 4-celled pollen-receptive stages in all backgrounds tested
272 (Figure S10B; (32, 33)). Consequently, we checked ROS levels in ovules at 20 HAE when ovules
273 are mature in all lines. Across three independent experiments, we confirmed that ROS levels are
274 significantly lower in *fer-4* ovules compared to wild-type (Figure 4B and S8C), indicating the that
275 ROS assay is functional in our hands and able to distinguish changes in ROS levels. However, we
276 found that ROS levels are consistently comparable to wild-type in mature ovules of *herk1 anj* and
277 *lre-5* (Figure 4B and S8C). To verify that the fertilisation defect is not rescued in the *herk1 anj* and
278 *lre-5* genotypes at 20 HAE, we confirmed that pollen tube overgrowth still occurs when ovules are
279 fertilised at this stage (Figure 4C). Taken together, these results suggest that FER acts upstream
280 of ROS accumulation in ovules prior to pollen tube arrival while, under our experimental conditions,

281 HERK1, ANJ and LRE are not required for this process. As these results conflict with a previous
282 study showing lower ROS levels in *lre-5* ovules (16), the function of LRE in ROS production may
283 be environment-dependent. Our results do not preclude that pollen tube arrival-induced ROS
284 signalling in the synergid cells is affected in *herk1 anj* and *lre-5*, however differences in transient
285 synergid-specific ROS burst cannot be quantified in our *in vitro* system.

286 **HERK1 and ANJEA interact with LORELEI**

287 LRE and its homolog LORELEI-LIKE GPI-ANCHORED PROTEIN 1 (LLG1) physically interact with
288 RLKs FER, FLAGELLIN SENSING 2 (FLS2) and EF-TU RECEPTOR (EFR) (15, 34). Mutations in
289 these GPI-anchored proteins and their associated RLKs result in similar phenotypes, with LRE and
290 LLG1 regarded as co-receptors and stabilisers of RLK function (15, 34). HERK1, ANJ and FER are
291 closely related RLKs and, given the similarities in reproduction defects and sub-cellular localisation
292 in synergid cells (Figure 3A), we hypothesised that HERK1 and ANJ may also act in complex with
293 LRE at the filiform apparatus. To this end, we used yeast two hybrid assays to test for direct
294 interactions between the extracellular juxtamembrane domains of HERK1 and ANJ (HERK1exJM,
295 ANJexJM) and LRE. Interactions between HERK1exJM and LRE, and ANJexJM and LRE were
296 detected, indicative of a possible direct interaction between these proteins (Figure 5A). To confirm
297 these interactions *in planta*, co-immunoprecipitation assays were performed in *Nicotiana*
298 *benthamiana* leaves after Agrobacterium-mediated transient expression of *pFER::HERK1-GFP*
299 and *p35S::HA-LRE*. HA-LRE co-immunprecipitated with HERK1-GFP (Figure 5B), confirming that
300 these two proteins form a complex *in planta*. We were unfortunately unable to detect ANJ-GFP or
301 ANJ-MYC expression in this heterologous system.

302 Additionally, we introduced the *lre-5* mutation into the *herk1 anj* background and characterised
303 fertility impairment in triple homozygous *herk1 anj lre-5* plants. No additive effect was observed in
304 the seed set defect in *herk1 anj lre-5* plants compared to *herk1 anj* and *lre-5* mutants (Figure 6A).
305 ROS production in these mutants was measured using $H_2$DCF-DA in *herk1 anj lre-5* ovules at 20
306 HAE. In agreement with the seed set phenotype, ROS levels were unaffected in the triple
307 homozygous line (Figure 6B). These results reinforce the hypothesis that HERK1, ANJ and LRE

act in the same signalling pathway and, given their cellular localisation and our protein-protein interaction results, we propose that HERK1-LRE and ANJ-LRE form part of a receptor complex in the filiform apparatus of synergid cells to mediate pollen tube reception.

## Discussion

Successful reproduction in angiosperms relies on tightly controlled communication between gametophytes where chemical and mechanical cues are exchanged (1). Here, we describe the role of the RLKs HERK1 and ANJ in early stages of fertilisation in Arabidopsis. HERK1 and ANJ are widely expressed in female reproductive tissues including the synergid cell area of ovules, where they are polarly localised in the filiform apparatus. *herk1 anj* plants fail to produce seeds from most ovules due to a maternally-derived pollen tube overgrowth defect. As female gametophytes develop normally in *herk1 anj* mutants, pollen tube overgrowth is likely due to impaired signalling. To clarify the position of HERK1/ANJ in relation to the previously characterised signalling elements of the pollen tube reception pathway, we have shown that NTA relocalisation after pollen tube reception is impaired in *herk1 anj* as described for FER, whereas ROS production at the micropylar entrance of ovules prior to pollen arrival is not affected. Interactions between HERK1/ANJ and LRE lead us to propose possible receptor complexes of HERK1-LRE and ANJ-LRE at the filiform apparatus.

Associated with diverse hormonal, developmental and stress responses, FER is regarded as a connective hub of cellular responses through its interactions with multiple partners, including small secreted peptides, cell-wall components, other RLKs, GPI-anchored proteins and ROPGEFs (15, 35-39). As related members of the CrRLK1L family, HERK1 and ANJ have the potential to perform similar roles to FER, as reported here in controlling pollen tube rupture. Interestingly, control of tip-growth in pollen tubes depends on two redundant pairs of CrRLK1Ls; ANX1 and ANX2, and BUPS1 and BUPS2 (8-11). ANX1/2 and BUPS1/2 form ANX-BUPS heterodimers to control pollen tube growth by sensing autocrine RALF signals (9). In turn, ovular RALFL34 efficiently induces pollen tube rupture at the pollen tip, likely through competition with autocrine RALFL4/19 (9). LEUCINE-RICH REPEAT EXTENSINS (LRXs) constitute an additional layer of regulation during

335 pollen tube growth (11). LRXs interact physically with RALFL4/19 and are thought to facilitate
336 RALFL sensing during pollen tube growth (11, 40). It is therefore possible to hypothesise that the
337 female control of pollen tube reception may also be executed via CrRLK1L heterocomplexes of
338 FER with either HERK1 or ANJ, which could sense pollen tube-derived cues to prime the female
339 gametophyte to trigger the required response to induce pollen tube rupture. Given the multiple
340 CrRLK1L-RALFL interactions identified to date (9, 11, 35, 41), pollen tube-produced RALF signals
341 constitute a potential candidate to induce synergid responses to pollen tube perception.
342 RALFL4/19 are continuously secreted at the growing tip of the pollen tube and while their
343 involvement in pollen growth has been thoroughly studied (9, 11), their possible dual role as
344 synergid-signalling activators remains unexplored. Disruption of synergid autocrine RALF
345 signalling upon pollen arrival constitutes another possible scenario, parallel to what is
346 hypothesised for RALFL34 and RALFL4/19 during pollen growth (9). Additionally, LRXs could
347 facilitate RALFL perception at the synergid cell to control pollen tube reception.

348 A second category of putative pollen tube cues involves changes in cell wall properties of the
349 filiform apparatus. As a polarised fast-growing structure, pollen tubes present cell walls that differ
350 from stationary cell types, with special emphasis on the growing tip where active cell wall
351 remodelling rapidly takes place (42). When the growing tip reaches the filiform apparatus, it
352 temporarily arrests growth, subsequently growing along the receptive synergid cell prior to rupture
353 (17). The prolonged direct physical contact between the growing tip and the filiform apparatus
354 likely allows a direct exchange of signals which could result in modification of the filiform apparatus
355 cell wall structure. CrRLK1L receptors present an extracellular malectin-like domain (43), a tandem
356 organisation of two malectin domains with structural similarity to the di-glucose binding malectin
357 protein (44). The malectin di-glucose binding residues are not conserved in the malectin-like
358 domains of ANX1/2 according to structural data (45, 46). However, direct interactions of FER,
359 ANX1/2 and BUPS1/2 malectin-like domains with the pectin building block polygalacturonic acid
360 have been recently reported (36, 47). An extracellular domain anchored to cell wall components
361 and a cytoplasmic kinase domain capable of inducing downstream signalling make FER and the
362 other CrRLK1L proteins a putative link between cell wall status and cellular responses (48).

363 Involvement of FER in root mechanosensing provides additional support for this hypothesis (49).
364 Therefore, FER and the related receptors HERK1 and ANJ may be fulfilling a cell wall integrity
365 surveillance function in the filiform apparatus, triggering cellular responses upon changes in the
366 composition or mechanical forces registered at this specialised cell wall structure. Future research
367 in this field will undoubtedly provide new views on how these RLKs integrate pollen-derived cues to
368 ensure tight control of fertilisation.

369 Receptor complexes are a common feature in signal transduction in multiple cellular processes
370 (50-52). Our genetic and biochemical results support a possible HERK1-LRE/ANJ-LRE
371 heterocomplex. LRE and related proteins form complexes with RLKs FER, FLS2 and EFR, making
372 them versatile co-receptors that mediate signal perception in multiple processes (15, 34). LRE
373 functions in the maternal control of fertilisation and early seed development (53, 54), whereas its
374 homolog LLG1 is restricted to vegetative growth and plant-pathogen interactions (34).
375 Uncharacterised LLG2 and LLG3 show pollen-specific expression in microarray data and therefore
376 constitute likely candidates as ANX1/2 and BUPS1/2 receptor complex partners to control pollen
377 tube growth. LRE proteins are thought to stabilise their receptor partners in the plasma membrane
378 and to act as direct co-receptors for the extracellular cues sensed by the RLK (15). As we found
379 that FER localisation in the filiform apparatus is unaltered in *lre-5* plants, as is HERK1/ANJ
380 localisation, our results do not support the role previously reported for LRE as a chaperone for
381 FER localisation in synergid cells (15). Nonetheless LRE could act as co-receptor for FER and
382 HERK1 or ANJ, forming tripartite HERK1-LRE-FER or ANJ-LRE-FER complexes that sense
383 pollen-derived ligands such as RALF peptides or cell wall components. Structural studies of RLK-
384 LRE complexes will shed light on LRE protein functions in membrane heterocomplexes.

385 Our results indicate that HERK1, ANJ and LRE are not required to generate the ROS-enriched
386 environment in the micropyle of mature ovules under our experimental conditions, while FER is
387 involved in this process (16). The role of FER in ROS production has also been characterised in
388 root hairs, where FER activates NADPH oxidase activity via ROPGEF and RAC/ROP GTPase
389 signalling, ensuring root hair growth stability (37). Micropylar ROS accumulation prior to pollen
390 tube arrival depends on NADPH oxidase activity and FER, suggesting a similar pathway to root

391 hairs may take place in synergid cells (16). This evidence places FER upstream of ROS
392 production, whereas FER, HERK1/ANJ and LRE would function upstream of pollen tube burst.
393 One possible explanation is that FER is a dual regulator in synergid cells, promoting ROS
394 production and regulating pollen tube reception, while HERK1/ANJ and LRE functions are
395 restricted to the latter under our environmental conditions. Kinase-dead mutants of FER rescue the
396 pollen tube overgrowth defect in *fer* mutants, but cannot restore the sensitivity to exogenous
397 RALF1 in root elongation (55). These recent findings support multiple signal transduction
398 mechanisms for FER in a context-dependent manner (55). It would thus be informative to test
399 whether the kinase-dead version of FER can restore the ovular ROS production defect in *fer*
400 mutants. The use of genetic ROS reporters expressed in synergid cells and pollen tubes in live
401 imaging experiments would allow us to observe specific changes in ROS production at the different
402 stages of pollen tube perception in ovules, as performed with $Ca^{2+}$ sensors (17, 29, 30). ROS
403 production and $Ca^{2+}$ pump activation in plant cells have been linked during plant-pathogen
404 interactions and are thought to take place during gametophyte communication (56, 57). Thus,
405 given the dynamic changes in $Ca^{2+}$ during the different stages of pollen tube reception in synergids
406 and pollen, it is likely that ROS production variations also take place in parallel. Studying ROS
407 production profiles during pollen perception in the *fer-4*, *herk1 anj* and *lre-5* backgrounds would
408 provide the resolution required to link these receptors to dynamic ROS regulation during pollen
409 reception. Induction of specific $Ca^{2+}$ signatures in the synergids upon pollen tube arrival is
410 dependent on FER, LRE and NTA (17). Given that NTA relocalisation after pollen reception
411 depends on functional HERK1/ANJ and NTA is involved in modulating $Ca^{+2}$ signatures in the
412 synergids, it is possible that HERK1 and ANJ might also be required for $Ca^{+2}$ signalling during
413 pollen perception.

414 Downstream signalling after pollen tube reception in the synergid cells likely involves interactions
415 of HERK1, ANJ and FER with cytoplasmic components through their kinase domain. Our results
416 indicate that the kinase activity of HERK1/ANJ is not required for controlling pollen tube rupture, as
417 has been reported for FER (26). The *fer-1* pollen tube overgrowth defect could also be rescued
418 with a chimeric protein comprising the FER extracellular domain and the HERK1 kinase domain

419 (26). This implies that the FER and HERK1/ANJ kinase domains are likely redundant in controlling
420 pollen tube burst and may transduce the signal in a similar manner. Testing whether FER-
421 dependent induction of ROS production in the micropyle is also independent of its kinase activity
422 and whether the HERK1/ANJ kinase domains can also substitute for the FER kinase domain in this
423 process would provide insight into how this signalling network is organised.

424 This study provides evidence for the involvement of multiple CrRLK1L receptors of pollen tube
425 perception at the female gametophyte and highlights the relevance of the CrRLK1Ls in controlling
426 reproduction in flowering plants.

# 427 Methods

## 428 Experimental Model and Subject Details

429 **Plant material.** *Arabidopsis thaliana* T-DNA insertion lines *herk1* (At3g46290; N657488; *herk1-1;*
430 (21)), and *anj* (At5g59700; N654842; *anj-1*) were obtained from the Nottingham Arabidopsis Stock
431 Centre (NASC;(58, 59)). T-DNA lines *fer-4* (At3g51550; N69044; (16, 35)) and *lre-5* (At4g26466;
432 N66102; (53)) were kindly provided by Prof. Alice Cheung (University of Massachusetts) and Dr.
433 Ravi Palanivelu (University of Arizona), respectively. Col-0 accession was used as wild-type in all
434 experiments. T-DNA lines were confirmed as homozygous for the T-DNA insertion by genotyping
435 PCR. The *anj* mutant line was characterised as a knockout of gene expression in this study by RT-
436 PCR.

437 **Growth conditions.** Seeds were stratified at 4ºC for three days. Seeds were sown directly on soil
438 and kept at high humidity for four days until seedlings emerged. Soil mix comprised a 4:1 (v:v)
439 mixture of Levington M3 compost:sand. Plants were grown in walk-in Conviron growth chambers
440 with 22ºC continuous temperature, 16 hours per day of ~120 $\mu mols^{-1}m^{-2}$ light and 60% humidity.
441 For selection of transformants, seeds were surface sterilised with chlorine gas, sown onto half-
442 strength Murashige and Skoog medium (MS; (60)), 0.8% (w/v) agar, pH 5.7 (adjusted with KOH),
443 supplemented with the appropriate antibiotic (25 µg/mL of hygromycin B or 50 µg/mL of
444 kanamycin). Seeds on plates were stratified for three days at 4ºC and then transferred to a growth

445 chamber (Snijders Scientific) at 22ºC, 16 hours per day of ~90 $\mu mols^{-1}m^{-2}$ of light. Basta selection
446 was carried out directly on soil soaked in a 1:1000 dilution of Whippet (150 g/L glufosinate
447 ammonium; AgChem Access Ltd).

448 **Method Details**

449 **Phenotyping.** To quantify seed production, fully expanded green siliques were placed on double-
450 sided sticky tape, valves were dissected along the replum with No. 5 forceps, exposing the
451 developing seeds. Dissected siliques were kept in a high humidity chamber until photographed to
452 avoid desiccation.

453 Carpels from self-pollinated or hand-pollinated flowers at stage 16 were selected for aniline blue
454 staining of pollen tubes. Carpels were fixed overnight in a 3:1 solution of ethanol:acetic acid, then
455 softened overnight in 8M NaOH, washed four times in water and incubated for three hours in
456 aniline blue staining solution (0.1% (w/v) aniline blue (Fisons Scientific) in 0.1M $K_2PO_4$-KOH buffer,
457 pH 11). Stained carpels were mounted in 50% glycerol, gently squashed onto the microscope slide
458 and then visualised with epifluorescence or confocal microscopy. Aniline blue fluorescence was
459 visualised in an epifluorescence microscope using a 400 nm LED light source and a filter set with
460 340-380 nm excitation, emission filter of 425 nm (long pass) and 400 nm dichroic mirror. Confocal
461 images were acquired using 403.5 nm laser line, 30.7 µm pinhole size and filter set with 405 nm
462 dichroic mirror and 525/50 nm emission filter cube.

463 Quick callose staining was carried out by incubating freshly dissected tissue samples in a 1000x
464 dilution of SR2200 (Renaissance Chemicals Ltd) in half-strength MS, 5% (w/v) sucrose, pH 5.7.
465 Samples were mounted in the staining solution directly and visualised under an epifluorescence
466 microscope with the same settings used for aniline blue staining. Callose-enriched structures like
467 pollen tubes and the filiform apparatus of ovules display a strong fluorescence within 10 minutes of
468 incubation. Only structures directly exposed to the SR2200 solution are stained.

469 To observe the development of the female gametophyte we used a confocal laser scanning
470 microscopy method as described by Christensen (61). Ovules were dissected from unpollinated

471 carpels, fixed for 2 hours in a 4% (v/v) solution of glutaraldehyde, 12.5mM sodium cacodylate
472 buffer pH 6.9, dehydrated in ethanol series (20%-100%, 20% intervals, 30 minutes each) and
473 cleared in a benzyl benzoate:benzyl alcohol 2:1 mixture for 2 hours prior to visualisation. Samples
474 were mounted in immersion oil, coverslips sealed with clear nail varnish and visualised with an
475 inverted confocal microscope. Fluorescence was visualised with 35.8 µm pinhole size, 642.4 nm
476 laser line and filter set of 640 nm dichroic mirror and 595/50 nm emission filter cube. Multiple z-
477 planes were taken and analysed with ImageJ.

478 Analyses of expression patterns of *HERK1* and *ANJ* were carried out by testing β-glucuronidase
479 activity in *promoter::GUS* reporter Col-0 plants from the T1 and T2 generations. Samples were
480 fixed in ice-cold 90% acetone for 20 minutes, then washed for 30 minutes in 50mM $NaPO_4$ buffer
481 pH 7.2. Samples were transferred to X-Gluc staining solution (2mM X-Gluc (Melford Laboratories
482 Ltd), 50mM $NaPO_4$ buffer pH 7.2, 2mM potassium ferrocyanide, 2mM potassium ferricyanide and
483 0.2% (v/v) Triton-X), vacuum-infiltrated for 30 minutes and incubated at 37ºC for several hours or
484 overnight. Samples were cleared in 75% ethanol and visualised under a light microscope or
485 stereomicroscope.

486 $H_2$DCF-DA staining of ROS in ovules was carried out as per (16). Ovules from unpollinated carpels
487 were dissected and incubated in staining solution (25µM $H_2$DCF-DA (Thermo Scientific), 50mM
488 KCl, 10mM MES buffer pH 6.15) for 15 minutes. Samples were subsequently washed three times
489 in $H_2$DCF-DA-free buffer for 5 minutes, mounted on slides and immediately visualised by
490 epifluorescence microscopy. $H_2$DCF-DA fluorescence was visualised using a 470 nm LED light
491 source and a filter set with 470/40 nm excitation filter, 460/50 nm emission filter and 495 nm
492 dichroic mirror.

493 All steps were performed at room temperature unless otherwise specified. Ovules were dissected
494 by placing carpels on double-sided sticky tape, separating the ovary walls from the replum with a
495 0.3 mm gauge needle, and by splitting the two halves of the ovary along the septum with No. 5
496 forceps. GFP was visualised by epifluorescence microscopy with the same settings used to

497 visualise $H_2$DCF-DA fluorescence. TdTomato was visualised using a 535 nm LED light source and
498 a filter set with 545/25 nm excitation filter, 605/70 nm emission filter and a 565 nm dichroic mirror.

499 **Cloning and transformation of Arabidopsis.** To study the cellular localisation and to
500 complement the pollen overgrowth defect we generated the constructs *pANJ::ANJ-GFP*,
501 *pHERK1::HERK1*, *pFER::FER-GFP, pANJ::ANJ-KD-GFP,* and *pHERK1::HERK1-KD*. Genomic
502 regions of interest (spanning 2 kb upstream of the start codon ATG and the full coding sequence
503 excluding stop codon) were amplified by PCR with Phusion DNA polymerase (NEB).
504 *Promoter::CDS* amplicons were cloned via KpnI/BamHI restriction sites into a pGreen-IIS
505 backbone (Basta resistance; from Detlef Weigel's group, Max Planck Institute for Developmental
506 Biology; (62)), with or without an in-frame C-terminal GFP coding sequence. Kinase-dead versions
507 of *HERK1* and *ANJ* were generated by targeted mutagenesis of the activation loop residues
508 D606N/K608R of ANJ and D609N/K611R of HERK1 using *pANJ::ANJ-GFP* and *pHERK1::HERK1*
509 constructs as template (63). To generate the GUS reporter constructs *pHERK1* and *pANJ* (2 kb
510 upstream of the ATG start codon) were cloned with a pENTR-dTOPO system (Thermo Scientific)
511 and then transferred to the GUS expression cassette in the pGWB433 destination vector via LR
512 recombination [LR clonase II; Thermo Scientific; (64)]. ASE *Agrobacterium tumefaciens* strain was
513 used with pGreen vectors; GV3101pMP90 strain was used otherwise. Arabidopsis stable
514 transformants were generated through the floral dip method. To test interaction *in vivo* in co-
515 immunoprecipitation assays, we generated GFP- and MYC-tagged overexpression constructs of
516 *HERK1*, *ANJ* and *FER*. PCR-amplified coding sequences were cloned into a pENTR-dTOPO
517 vector and then transferred to the destination vectors pGWB405 and pGWB420 [*35S::gene-GFP*;
518 *35S::gene-MYC* cassettes, respectively; (64)] via LR recombination. To test direct interaction
519 between HERK1exJM, ANJexJM and LRE in yeast, we cloned the extracellular juxtamembrane
520 sequence corresponding to the 81 amino acids N-terminal of the predicted transmembrane domain
521 of HERK1 and ANJ, as well as the sequence corresponding to the aminoacids 23-138 of LRE [as
522 per (15)]. Amplicons were cloned into yeast two hybrid vectors pGADT7 and pGBKT7 via SmaI
523 restriction digests, in frame with the activation or DNA binding domains (AD or BD, respectively).

524 Col-0 genomic DNA was used as the template for all cloning events unless otherwise specified.
525 Primers used for cloning are listed in Supplementary Table S2.

526 **Genotyping and RT-PCR.** Genotyping PCRs were performed with Taq polymerase and 35 cycles
527 with 60ºC annealing temperature and one minute extension time. Genomic DNA was extracted
528 from leaves of 2 week old seedlings by grinding fresh tissue in DNA extraction buffer (200mM Tris-
529 HCl pH 7.5, 250mM NaCl, 25mM EDTA and 0.5% SDS), precipitating DNA with isopropanol,
530 washing pellets with 75% EtOH and resuspending DNA in water. RNA was extracted with E.Z.N.A.
531 plant RNA extraction kit (Omega Bio-Tek) from 100 mg of floral tissue from multiple plants per line.
532 RNA concentrations were normalised, an aliquot was DNaseI-treated and subsequently
533 transcribed into first strand cDNA with the RevertAid cDNA synthesis kit (Thermo Scientific) using
534 random hexamers. RT-PCR of *ANJ* and the control gene *FER* were performed with the conditions
535 used in genotyping PCRs with 45 seconds of extension time. Primers for genotyping and RT-PCR
536 are listed in the Supplementary Table S2.

537 **Yeast two-hybrid.** Direct interaction assays in yeast were carried out following the Clontech small-
538 scale LiAc yeast transformation procedure. Yeast strain Y187 was transformed with pGADT7
539 constructs and yeast strain Y2HGold with pGBKT7 constructs (including empty vectors as
540 controls). Yeast diploids cells carrying both plasmids were obtained by mating and interaction test
541 were surveyed on selective media lacking leucine, tryptophan and histidine.

542 **Co-immunoprecipitation and western blot.** *N. benthamiana* leaves were infiltrated with *A.*
543 *tumefaciens* strain GV3101 carrying constructs indicated in figure captions. In all cases, leaves
544 were co-infiltrated with *A. tumefaciens* carrying a P19 silencing suppressor. Leaves were
545 harvested 2 days post-infiltration and frozen in liquid nitrogen before extraction in buffer (20 mM
546 MES pH 6.3, 100 mM NaCl, 10% glycerol, 2 mM EDTA, 5 mM DTT, supplemented with 1%
547 IGEPAL and protease inhibitors). Immunoprecipitations were performed in the same buffer with
548 0.5% IGEPAL for 4 hours at 4ºC with GFP-trap (Chromotek) or Anti-HA Affinity Matrix (Roche)
549 resin. Beads were washed with the same buffer and bound proteins were eluted by addition of
550 SDS loading dye and heating to 90ºC for 10 min. Proteins were separated by SDS-PAGE and

551 detected via Western blot following blocking (in TBS-0.1% Tween-20 with 5% non-fat milk powder)
552 with the following antibody dilutions: α-GFP-HRP (B-2, Santa Cruz), 1:5000; α-HA-HRP (3F10,
553 Roche), 1:3000.

554 **Microscopy and image building.** Epifluorescence images were obtained with Leica DM6 or
555 Olympus BX51 widefield microscopes equipped with HC PL Fluotar objectives or UPlanFl 4x,10x
556 and 20x objectives, respectively. A Nikon A1 inverted confocal laser scanning microscope fitted
557 with Plan Fluor 40x oil and Plan Apo VC 60x oil objectives was used to obtain confocal
558 micrographs. A Leica M165 FC stereomicroscope was used to visualise floral tissues from GUS
559 stained samples. Leica LASX, NIS Elements Viewer and ImageJ software were used to analyse
560 microscopy images. Inkscape was used to build all figures in this article.

561 **Quantification and Statistical Analysis**

562 Leica LASX software was used to obtain relative fluorescence intensity profiles from synergid cells
563 by defining linear regions of interest across the synergid cytoplasm in a micropylar to chalazal
564 orientation. Synergid cytoplasm area was defined between filiform apparatus and the synergid-egg
565 cell chalazal limit using the corresponding DIC images.

566 Statistical significance in seed set averages and relative fluorescence averages (at equivalent
567 distances from the filiform apparatus) were assessed with Student's *t*-tests. $\chi$-square tests were
568 used to compare distributions obtained in pollen tube overgrowth assays and ROS measurements
569 in ovules, using the distribution obtained in wild-type plants as the expected distribution. In all
570 tests, *$p<0.05$, **$p<0.01$, and ***$p<0.001$. Sample size *n* is indicated in the graphs or figure
571 legends.

572 **Acknowledgements**

573 S. G-T. was supported by a Department of Animal and Plant Sciences postgraduate teaching
574 fellowship. Research in J.G.'s lab is supported by RCUK grant BB/N004167/1. T. A. D. was
575 supported by a long-term post-doctoral fellowship from the European Molecular Biology

576 Organisation (LTF 100-2017). N. B-T. was supported by a MINECO FPI Fellowship (BES-2014-
577 068868) and we acknowledge David Alabadi for his supervision of N. B-T. The Zipfel laboratory
578 was supported by the Gatsby Charitable Foundation and European Research Council (PEPTALK).
579 We thank Andrew Fleming and his group at the University of Sheffield for early feedback and
580 guidance on experiments, Alice Cheung and Qiaohong Duan from the University of Massachusetts
581 for advice on the ROS assays and for sharing *fer-4* seeds with us, Chao Li from East China
582 Normal University for the *p35S::HA-LRE* construct, Ravi Palanivelu from the University of Arizona
583 for *lre-5* seeds, Martin Bayer from the Max Planck Institute for Developmental Biology for the
584 *pLAT52::TdTomato* line, Ueli Grossniklaus from the University of Zurich for the *pFER::HERK1-*
585 *GFP* and *pLRE::LRE-Citrine* constructs and Sharon Kessler from Purdue University for sharing the
586 *pMYB98::NTA-GFP* construct.

587

588 **Declaration of interests**

589 The authors declare no competing interests.

590 **References**

591 1. Dresselhaus T, Sprunck S, Wessel GM. Fertilization Mechanisms in Flowering Plants.
592 Current Biology. 2016;26(3):R125-R39.
593 2. Higashiyama T. The synergid cell: attractor and acceptor of the pollen tube for double
594 fertilization. Journal of Plant Research. 2002;115(1118):149-60.
595 3. Huang B-Q, Russell SD. Female Germ Unit: Organization, Isolation, and Function. In: Russell
596 SD, Dumas C, editors. International Review of Cytology. 140: Academic Press; 1992. p. 233-93.
597 4. Okuda S, Tsutsui H, Shiina K, Sprunck S, Takeuchi H, Yui R, et al. Defensin-like polypeptide
598 LUREs are pollen tube attractants secreted from synergid cells. Nature. 2009;458(7236):357-61.
599 5. Wang T, Liang L, Xue Y, Jia PF, Chen W, Zhang MX, et al. A receptor heteromer mediates
600 the male perception of female attractants in plants. Nature. 2016;531(7593):241-4.
601 6. Takeuchi H, Higashiyama T. Tip-localized receptors control pollen tube growth and LURE
602 sensing in Arabidopsis. Nature. 2016;531(7593):245-8.
603 7. Zhang XX, Liu WJ, Nagae TT, Takeuchi H, Zhang HQ, Han ZF, et al. Structural basis for
604 receptor recognition of pollen tube attraction peptides. Nature Communications. 2017;8:1331.
605 8. Boisson-Dernier A, Roy S, Kritsas K, Grobei MA, Jaciubek M, Schroeder JI, et al. Disruption
606 of the pollen-expressed FERONIA homologs ANXUR1 and ANXUR2 triggers pollen tube discharge.
607 Development. 2009;136(19):3279-88.

608 9. Ge ZX, Bergonci T, Zhao YL, Zou YJ, Du S, Liu MC, et al. Arabidopsis pollen tube integrity and
609 sperm release are regulated by RALF-mediated signaling. Science. 2017;358(6370):1596-9.
610 10. Miyazaki S, Murata T, Sakurai-Ozato N, Kubo M, Demura T, Fukuda H, et al. ANXUR1 and 2,
611 sister genes to FERONIA/SIRENE, are male factors for coordinated fertilization. Curr Biol.
612 2009;19(15):1327-31.
613 11. Mecchia MA, Santos-Fernandez G, Duss NN, Somoza SC, Boisson-Dernier A, Gagliardini V,
614 et al. RALF4/19 peptides interact with LRX proteins to control pollen tube growth in Arabidopsis.
615 Science. 2017;358(6370):1600-3.
616 12. Schoenaers S, Balcerowicz D, Costa A, Vissenberg K. The Kinase ERULUS Controls Pollen
617 Tube Targeting and Growth in Arabidopsis thaliana. Frontiers in Plant Science. 2017;8:1942.
618 13. Huck N, Moore JM, Federer M, Grossniklaus U. The Arabidopsis mutant feronia disrupts
619 the female gametophytic control of pollen tube reception. Development. 2003;130(10):2149-59.
620 14. Escobar-Restrepo JM, Huck N, Kessler S, Gagliardini V, Gheyselinck J, Yang WC, et al. The
621 FERONIA receptor-like kinase mediates male-female interactions during pollen tube reception.
622 Science. 2007;317(5838):656-60.
623 15. Li C, Yeh FL, Cheung AY, Duan Q, Kita D, Liu MC, et al. Glycosylphosphatidylinositol-
624 anchored proteins as chaperones and co-receptors for FERONIA receptor kinase signaling in
625 Arabidopsis. Elife. 2015;4:e06587.
626 16. Duan Q, Kita D, Johnson EA, Aggarwal M, Gates L, Wu HM, et al. Reactive oxygen species
627 mediate pollen tube rupture to release sperm for fertilization in Arabidopsis. Nat Commun.
628 2014;5:3129.
629 17. Ngo QA, Vogler H, Lituiev DS, Nestorova A, Grossniklaus U. A Calcium Dialog Mediated by
630 the FERONIA Signal Transduction Pathway Controls Plant Sperm Delivery. Developmental Cell.
631 2014;29(4):491-500.
632 18. Kessler SA, Shimosato-Asano H, Keinath NF, Wuest SE, Ingram G, Panstruga R, et al.
633 Conserved molecular components for pollen tube reception and fungal invasion. Science.
634 2010;330(6006):968-71.
635 19. Jones DS, Kessler SA. Cell type-dependent localization of MLO proteins. Plant Signaling &
636 Behavior. 2017;12(11):e1393135.
637 20. Galindo-Trigo S, Gray JE, Smith LM. Conserved Roles of CrRLK1L Receptor-Like Kinases in
638 Cell Expansion and Reproduction from Algae to Angiosperms. Front Plant Sci. 2016;7:1269.
639 21. Guo H, Li L, Ye H, Yu X, Algreen A, Yin Y. Three related receptor-like kinases are required for
640 optimal cell elongation in Arabidopsis thaliana. Proc Natl Acad Sci U S A. 2009;106(18):7648-53.
641 22. Guo H, Ye H, Li L, Yin Y. A family of receptor-like kinases are regulated by BES1 and involved
642 in plant growth in Arabidopsis thaliana. Plant Signal Behav. 2009;4(8):784-6.
643 23. Capron A, Gourgues M, Neiva LS, Faure J-E, Berger F, Pagnussat G, et al. Maternal Control
644 of Male-Gamete Delivery in Arabidopsis Involves a Putative GPI-Anchored Protein Encoded by the
645 LORELEI Gene. The Plant Cell. 2008;20(11):3038-49.
646 24. Beale KM, Leydon AR, Johnson MA. Gamete Fusion Is Required to Block Multiple Pollen
647 Tubes from Entering an Arabidopsis Ovule. Current Biology. 2012;22(12):1090-4.
648 25. Maruyama D, Volz R, Takeuchi H, Mori T, Igawa T, Kurihara D, et al. Rapid Elimination of
649 the Persistent Synergid through a Cell Fusion Mechanism. Cell. 2015;161(4):907-18.
650 26. Kessler SA, Lindner H, Jones DS, Grossniklaus U. Functional analysis of related CrRLK1L
651 receptor-like kinases in pollen tube reception. EMBO Rep. 2015;16(1):107-15.
652 27. Knighton DR, Zheng JH, Teneyck LF, Ashford VA, Xuong NH, Taylor SS, et al. Crystal-
653 Structure of the Catalytic Subunit of Cyclic Adenosine-Monophosphate Dependent Protein-Kinase.
654 Science. 1991;253(5018):407-14.

655 28. Tsukamoto T, Qin Y, Huang YD, Dunatunga D, Palanivelu R. A role for LORELEI, a putative
656 glycosylphosphatidylinositol-anchored protein, in Arabidopsis thaliana double fertilization and
657 early seed development. Plant Journal. 2010;62(4):571-88.
658 29. Hamamura Y, Nishimaki M, Takeuchi H, Geitmann A, Kurihara D, Higashiyama T. Live
659 imaging of calcium spikes during double fertilization in Arabidopsis. Nature Communications.
660 2014;5:4722.
661 30. Denninger P, Bleckmann A, Lausser A, Vogler F, Ott T, Ehrhardt DW, et al. Male-female
662 communication triggers calcium signatures during fertilization in Arabidopsis. Nature
663 Communications. 2014;5:4645.
664 31. Smyth DR, Bowman JL, Meyerowitz EM. Early Flower Development in Arabidopsis. Plant
665 Cell. 1990;2(8):755-67.
666 32. Christensen CA, Subramanian S, Drews GN. Identification of gametophytic mutations
667 affecting female gametophyte development in Arabidopsis. Developmental Biology.
668 1998;202(1):136-51.
669 33. Yadegari R, Drews GN. Female gametophyte development. Plant Cell. 2004;16:S133-S41.
670 34. Shen QJ, Bourdais G, Pan HR, Robatzek S, Tang DZ. Arabidopsis
671 glycosylphosphatidylinositol-anchored protein LLG1 associates with and modulates FLS2 to
672 regulate innate immunity. P Natl Acad Sci USA. 2017;114(22):5749-54.
673 35. Haruta M, Sabat G, Stecker K, Minkoff BB, Sussman MR. A peptide hormone and its
674 receptor protein kinase regulate plant cell expansion. Science. 2014;343(6169):408-11.
675 36. Feng W, Kita D, Peaucelle A, Cartwright HN, Doan V, Duan QH, et al. The FERONIA Receptor
676 Kinase Maintains Cell-Wall Integrity during Salt Stress through Ca2+ Signaling. Current Biology.
677 2018;28(5):666-75.
678 37. Duan Q, Kita D, Li C, Cheung AY, Wu HM. FERONIA receptor-like kinase regulates RHO
679 GTPase signaling of root hair development. Proc Natl Acad Sci U S A. 2010;107(41):17821-6.
680 38. Stegmann M, Monaghan J, Smakowska-Luzan E, Rovenich H, Lehner A, Holton N, et al. The
681 receptor kinase FER is a RALF-regulated scaffold controlling plant immune signaling. Science.
682 2017;355(6322):287-9.
683 39. Hou YN, Guo XY, Cyprys P, Zhang Y, Bleckmann A, Cai L, et al. Maternal ENODLs Are
684 Required for Pollen Tube Reception in Arabidopsis. Current Biology. 2016;26(17):2343-50.
685 40. Stegmann M, Zipfel C. Complex regulation of plant sex by peptides. Science.
686 2017;358(6370):1544-5.
687 41. Gonneau M, Desprez T, Martin M, Doblas VG, Bacete L, Miart F, et al. Receptor Kinase
688 THESEUS1 Is a Rapid Alkalinization Factor 34 Receptor in Arabidopsis. Current Biology.
689 2018;28(15):2452-8.
690 42. Chebli Y, Kaneda M, Zerzour R, Geitmann A. The Cell Wall of the Arabidopsis Pollen Tube-
691 Spatial Distribution, Recycling, and Network Formation of Polysaccharides. Plant Physiology.
692 2012;160(4):1940-55.
693 43. Boisson-Dernier A, Kessler SA, Grossniklaus U. The walls have ears: the role of plant
694 CrRLK1Ls in sensing and transducing extracellular signals. J Exp Bot. 2011;62(5):1581-91.
695 44. Schallus T, Jaeckh C, Feher K, Palma AS, Liu Y, Simpson JC, et al. Malectin: a novel
696 carbohydrate-binding protein of the endoplasmic reticulum and a candidate player in the early
697 steps of protein N-glycosylation. Mol Biol Cell. 2008;19(8):3404-14.
698 45. Du S, Qu LJ, Xiao J. Crystal structures of the extracellular domains of the CrRLK1L receptor-
699 like kinases ANXUR1 and ANXUR2. Protein Sci. 2018;27(4):886-92.
700 46. Moussu S, Augustin S, Roman AO, Broyart C, Santiago J. Crystal structures of two tandem
701 malectin-like receptor kinases involved in plant reproduction. Acta Crystallogr D Struct Biol.
702 2018;74(Pt 7):671-80.

703 47. Lin W, Tang W, Anderson C, Yang Z. FERONIA's sensing of cell wall pectin activates ROP
704 GTPase signaling in Arabidopsis. bioRxiv. 2018.
705 48. Verger S, Hamant O. Plant Physiology: FERONIA Defends the Cell Walls against Corrosion.
706 Curr Biol. 2018;28(5):R215-R7.
707 49. Shih HW, Miller ND, Dai C, Spalding EP, Monshausen GB. The Receptor-like Kinase FERONIA
708 Is Required for Mechanical Signal Transduction in Arabidopsis Seedlings. Current Biology.
709 2014;24(16):1887-92.
710 50. Greeff C, Roux M, Mundy J, Petersen M. Receptor-like kinase complexes in plant innate
711 immunity. Frontiers in Plant Science. 2012;3:209.
712 51. Burkart RC, Stahl Y. Dynamic complexity: plant receptor complexes at the plasma
713 membrane. Current Opinion in Plant Biology. 2017;40:15-21.
714 52. Couto D, Zipfel C. Regulation of pattern recognition receptor signalling in plants. Nature
715 Reviews Immunology. 2016;16:537.
716 53. Tsukamoto T, Qin Y, Huang Y, Dunatunga D, Palanivelu R. A role for LORELEI, a putative
717 glycosylphosphatidylinositol-anchored protein, in Arabidopsis thaliana double fertilization and
718 early seed development. The Plant Journal. 2010;62(4):571-88.
719 54. Wang YB, Tsukamoto T, Noble JA, Liu XL, Mosher RA, Palanivelu R. Arabidopsis LORELEI, a
720 Maternally Expressed Imprinted Gene, Promotes Early Seed Development. Plant Physiology.
721 2017;175(2):758-73.
722 55. Haruta M, Gaddameedi V, Burch H, Fernandez D, Sussman MR. Comparison of the effects
723 of a kinase-dead mutation of FERONIA on ovule fertilization and root growth of Arabidopsis. FEBS
724 Lett. 2018.
725 56. Bleckmann A, Alter S, Dresselhaus T. The beginning of a seed: regulatory mechanisms of
726 double fertilization. Frontiers in Plant Science. 2014;5:452.
727 57. Ma W, Berkowitz GA. The grateful dead: calcium and cell death in plant innate immunity.
728 Cell Microbiol. 2007;9(11):2571-85.
729 58. Alonso JM, Stepanova AN, Leisse TJ, Kim CJ, Chen HM, Shinn P, et al. Genome-wide
730 Insertional mutagenesis of Arabidopsis thaliana. Science. 2003;301(5633):653-7.
731 59. Kleinboelting N, Huep G, Kloetgen A, Viehoever P, Weisshaar B. GABI-Kat SimpleSearch:
732 new features of the Arabidopsis thaliana T-DNA mutant database. Nucleic Acids Research.
733 2012;40(D1):D1211-D5.
734 60. Murashige T, Skoog F. A Revised Medium for Rapid Growth and Bio Assays with Tobacco
735 Tissue Cultures. Physiologia Plantarum. 1962;15(3):473-97.
736 61. Christensen CA, King EJ, Jordan JR, Drews GN. Megagametogenesis in Arabidopsis wild type
737 and the Gf mutant. Sex Plant Reprod. 1997;10(1):49-64.
738 62. Mathieu J, Warthmann N, Kuttner F, Schmid M. Export of FT protein from phloem
739 companion cells is sufficient for floral induction in Arabidopsis. Current Biology. 2007;17(12):1055-
740 60.
741 63. Ho SN, Hunt HD, Horton RM, Pullen JK, Pease LR. Site-Directed Mutagenesis by Overlap
742 Extension Using the Polymerase Chain-Reaction. Gene. 1989;77(1):51-9.
743 64. Nakagawa T, Suzuki T, Murata S, Nakamura S, Hino T, Maeo K, et al. Improved Gateway
744 Binary Vectors: High-Performance Vectors for Creation of Fusion Constructs in Transgenic Analysis
745 of Plants. Bioscience, Biotechnology, and Biochemistry. 2007;71(8):2095-100.
746

747

748 **Figures**

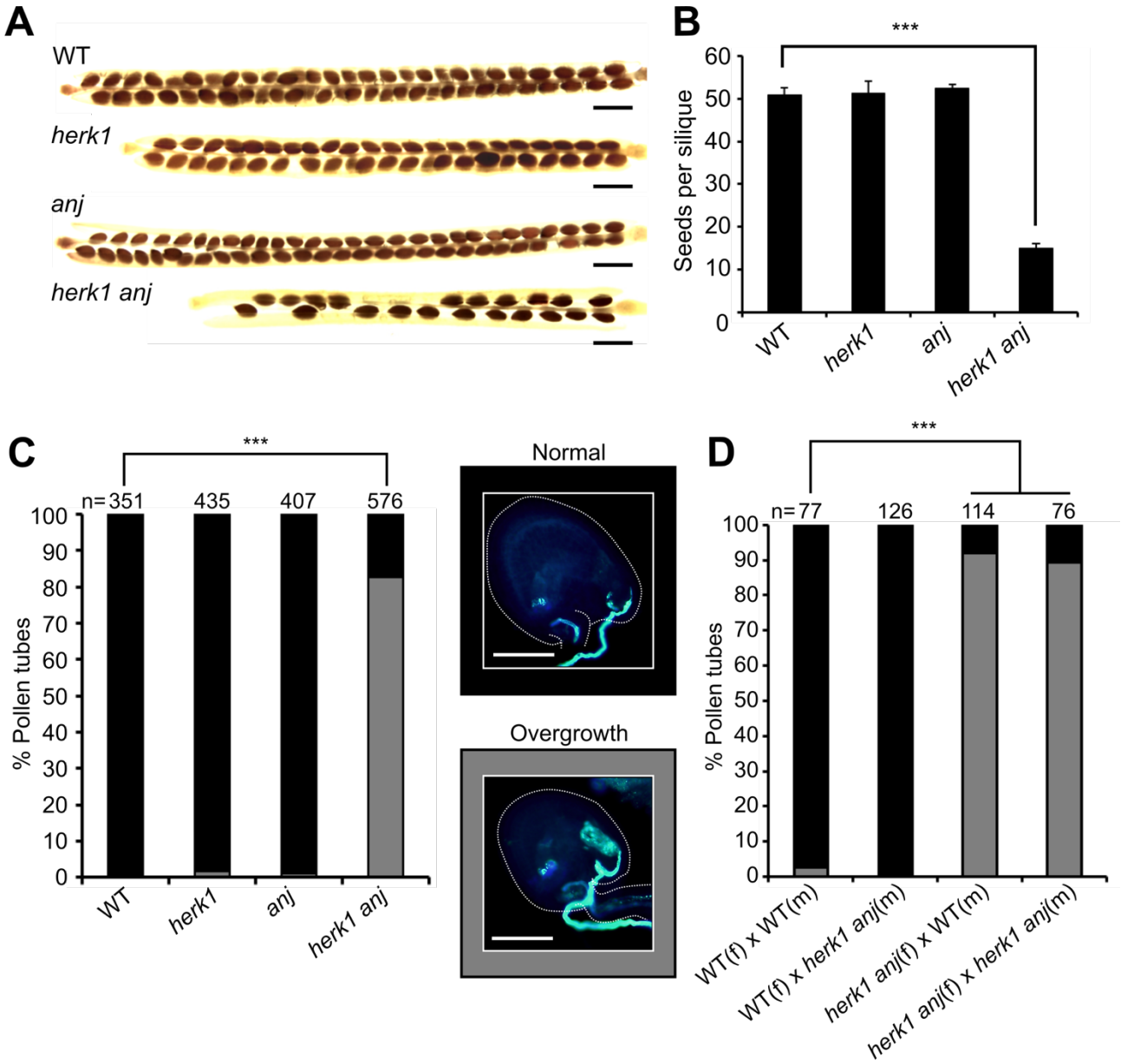


749

750

751 **Figure 1. The *herk1 anj* fertility defect is caused by maternally-mediated pollen tube**
752 **overgrowth.** (A) Representative mature siliques from wild-type (WT; Col-0), *herk1*, *anj* and *herk1*
753 *anj* plants. Siliques were collected prior to dehiscence and cleared in 0.4M NaOH, 1% Triton X-
754 100. Scale bar = 1 mm. (B) Developing seeds per silique in wild-type, *herk1*, *anj* and *herk1 anj*
755 plants. Fully expanded siliques were dissected and photographed under a stereomicroscope. *n* =
756 15 (four independent experiments with at least three plants per line and five siliques per plant).

757 Data presented are means ± SEM. *** $p<0.001$ (Student's *t*-test). (C) Percentage of pollen tubes
758 with normal reception at the female gametophyte (black bars) and with overgrowth (grey bars) as
759 assessed by aniline blue staining. 15 self-pollinated stage 16 flowers from wild-type, *herk1*, *anj* and
760 *herk1 anj* were analysed. Legend scale bars = 50 µm. *** $p<0.001$ ($\chi$-square tests). (D) Aniline
761 blue staining of pollen tube reception in reciprocal crosses between wild-type and *herk1 anj* plants
762 with at least two siliques per cross. Legend as per (C). *** $p<0.001$ ($\chi$-square tests).

763

764

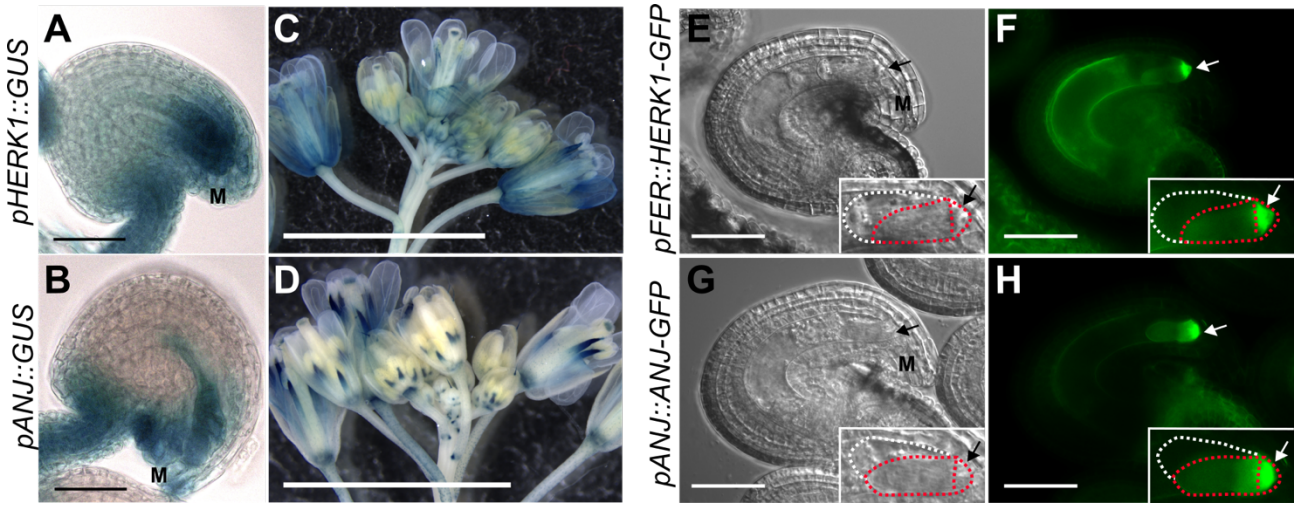


**Figure 2. HERK1 and ANJ are expressed in the female gametophyte and localise to the filiform apparatus of the synergid cells.** (A-B) Expression of *pHERK1::GUS* and *pANJ::GUS* in mature ovules. Scale bars = 25 µm. (C-D) Expression of *pHERK1::GUS* and *pANJ::GUS* in inflorescences. Scale bars = 5 mm. (E,F) Localisation of HERK1-GFP in the synergid cell from the *pFER::HERK1-GFP* construct in (F) and corresponding differential interference contrast (DIC) image in (E). White and red dotted lines delineate the egg cell and synergid cells, respectively. Scale bars = 50 µm. (G,H) Localisation of ANJ-GFP in the synergid cell from the *pANJ::ANJ-GFP* construct in (H) and corresponding DIC image in (G). White and red dotted lines delineate the egg cell and synergid cells, respectively. Scale bars = 50 µm. M, micropyle. Arrows, filiform apparatus.

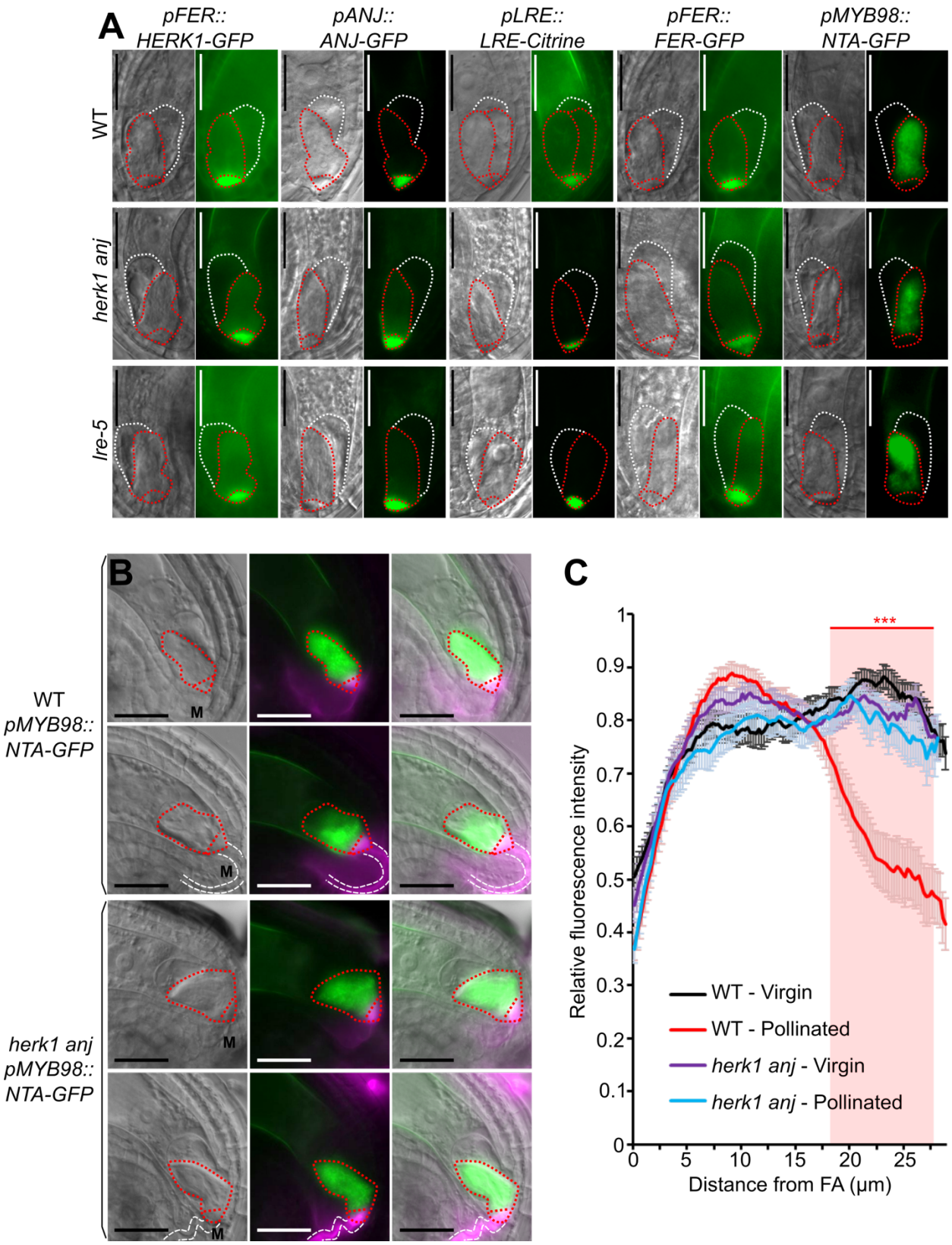


**Figure 3. Normal synergid localisation of HERK1, ANJ, LRE, FER and NTA pre-fertilisation and impaired relocalisation of NTA after pollen tube reception in *herk1 anj*.** (A) Localisation of HERK1, ANJ, LRE, FER and NTA in the synergid cell of wild-type (Col-0; WT), *herk1 anj* and *lre-5*

782 in unfertilised ovules, as shown by *pFER::HERK1-GFP*, *pANJ::ANJ-GFP*, *pLRE::LRE-Citrine*,
783 *pFER::FER-GFP* and *pMYB98::NTA-GFP*. DIC and fluorescence images are shown, left to right,
784 respectively. White and red dotted lines delineate the egg cell and synergid cells, respectively.
785 Scale bars = 25 µm. (B) Localisation of NTA in the synergid cell of wild-type and *herk1 anj* plants
786 before (upper panels) and after (lower panels) pollen tube arrival. In green, NTA localisation as
787 shown by *pMYB98::NTA-GFP* fluorescence. In magenta, callose of the filiform apparatus and
788 pollen tube stained with SR2200. From left to right, images shown are DIC, merged fluorescence
789 images, and merged images of DIC and fluorescence. White and red dotted lines delineate the
790 pollen tube and synergid cells, respectively. Scale bars = 25 µm. M, micropyle. (C) Profile of
791 relative fluorescence intensity of NTA-GFP along the synergid cells of wild-type and *herk1 anj*
792 ovules, before (virgin) and after (pollinated) pollen arrival. Data shown are means ± SEM, n = 25.
793 *** $p<0.001$ (Student's *t*-test). FA, filiform apparatus.

794

795

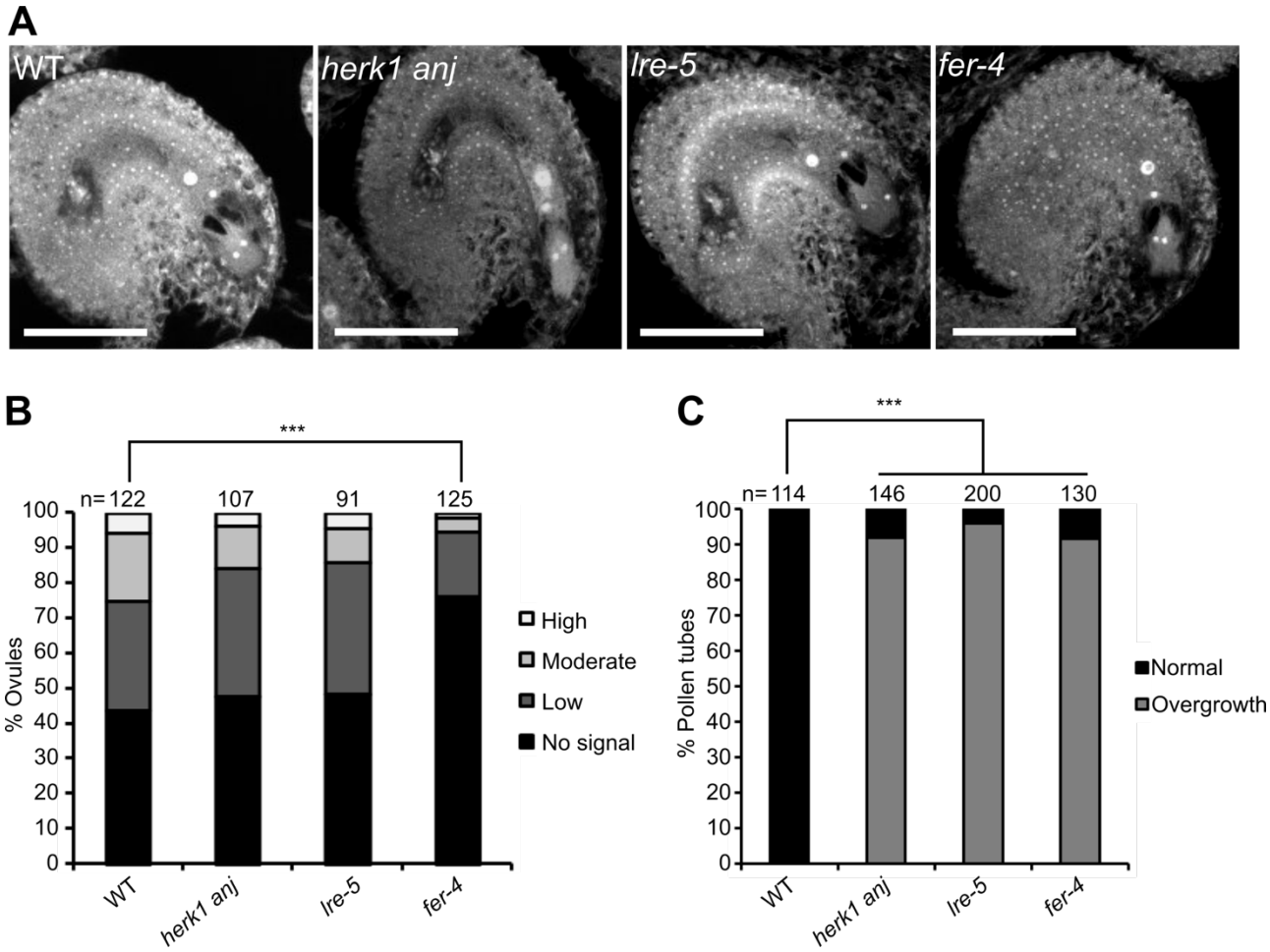


**Figure 4. *herk1 anj* mature female gametophytes are morphologically normal and unaffected in ROS production at the micropyle.** (A) Representative images of ovules from wild-type, *herk1 anj*, *lre-5* and *fer-4* 20 HAE displaying the mature female gametophyte structure. Images presented here are maximum intensity projections from confocal microscopy images across several z-planes of ovules stained as per (61). Scale bars = 50 µm. (B) Quantification of $H_2$CDF-DA staining of ROS in ovules from wild-type, *herk1 anj*, *lre-5* and *fer-4* plants at 20 HAE. Categories are listed in the legend (see also Figure S8A). Ovules dissected from at least five siliques per line. *** $p<0.001$ ($\chi$-square tests). (C) Percentage of pollen tubes with normal reception at the female gametophyte (black bars) and displaying overgrowth (grey bars) in wild-type, *herk1 anj*, *lre-5* and *fer-4* plants, manually selfed at 20 HAE. Fertilisation events counted from at least three siliques per line. *** $p<0.001$ (Student's *t*-test).

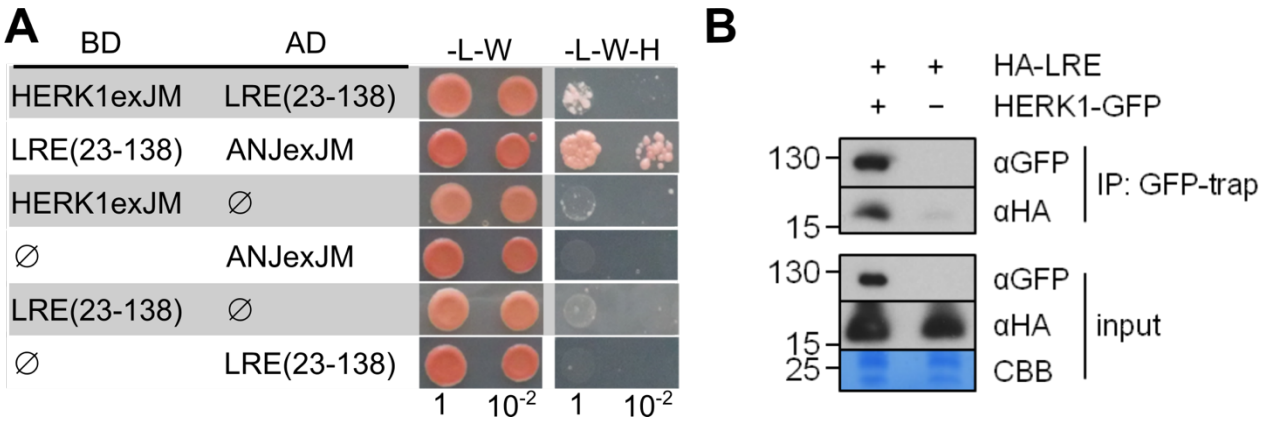


**Figure 5. HERK1 and ANJ interact with LRE.** (A) Yeast two hybrid assays of the extracellular juxtamembrane domains of HERK1 and ANJ (HERK1exJM and ANJexJM, respectively) with LRE (residues 23-138; signal peptide and C-terminal domains excluded). Ø represents negative controls where no sequence was cloned into the activating domain (AD) or DNA-binding domain (BD) constructs. -L-W-H, growth medium depleted of leucine (-L), tryptophan (-W) and histidine (-H). (B) Co-immunoprecipitation of HA-LRE with HERK1-GFP following 2 days of transient expression in *N. benthamiana* leaves. Numbers indicate MW marker sizes in kDa. Assays were performed twice with similar results.

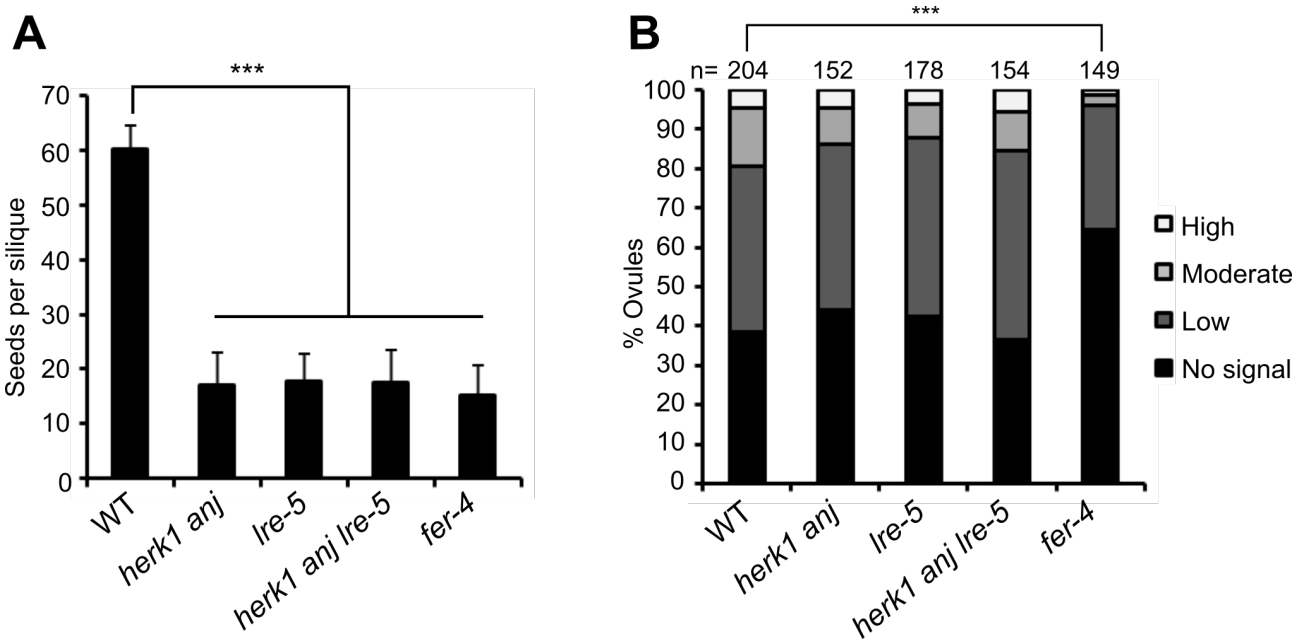


**Figure 6. HERK1, ANJ and LRE do not act additively in seed set or ROS production.** (A) Quantification of developing seeds per silique in wild-type, *herk1 anj*, *lre-5*, *herk1 anj lre-5* and *fer-4* plants. Fully expanded siliques were dissected and photographed under a stereomicroscope. n = 25. Data presented are means ± SD. *** $p<0.001$ (Student's *t*-test). (B) Quantification of the $H_2$CDF-DA staining of ROS in ovules from wild-type, *herk1 anj*, *lre-5*, *herk1 anj lre-5* and *fer-4* plants at 20 HAE. Categories are listed in the legend (see also Figure S8A). Ovules dissected from at least five siliques per line. *** $p<0.001$ ($\chi$-square tests).